

OPEN

Zinc phthalocyanines as light harvesters for SnO₂-based solar cells: a case study

Riccardo Milan^{1,2}, Gurpreet Singh Selopal^{1,3,4}, Marco Cavazzini⁵, Simonetta Orlandi⁵, Rita Boaretto⁶, Stefano Caramori⁶, Isabella Concina^{1,2,7*} & Gianluca Pozzi^{5*}

SnO₂ nanoparticles have been synthesized and used as electron transport material (ETM) in dye sensitized solar cells (DSSCs), featuring two peripherally substituted push-pull zinc phthalocyanines (ZnPcs) bearing electron donating diphenylamine substituents and carboxylic acid anchoring groups as light harvesters. These complexes were designed on the base of previous computational studies suggesting that the integration of secondary amines as donor groups in the structure of unsymmetrical ZnPcs might enhance photovoltaics performances of DSSCs. In the case of TiO₂-based devices, this hypothesis has been recently questioned by experimental results. Herein we show that the same holds for SnO₂, despite the optimal matching of the optoelectronic characteristics of the synthesized nanoparticles and diphenylamino-substituted ZnPcs, thus confirming that other parameters heavily affect the solar cells performances and should be carefully taken into account when designing materials for photovoltaic applications.

In spite of the loss of fame following the advent of perovskite solar cells, dye sensitized solar cells (DSSCs), which can be manufactured from eco-friendly, low-cost materials, still deserve attention due to the careful materials engineering and coupling they are the object of, asking scientists of different fields to join efforts to shine light on basic phenomena. Major efforts in DSSCs are still devoted to cell components engineering^{1,2}, including the seek for wide band gap semiconducting metal oxides (MOx) as electron transport materials (ETM) alternative to TiO₂¹⁻⁶, and to the development of new photosensitizers enabling the exploitation of a wider portion of the solar spectrum⁷. Investigations should be then focused not only to enhance the overall functional performances of the solar energy converting devices, which are so far limited, but especially to unveil fundamental phenomena and processes.

In the field of ETMs to be used as photoanodes in DSSCs, SnO₂ is an interesting candidate, assuming that a material-by-design approach is adopted in the preparation of nanostructures featuring proper optoelectronic characteristics, such as light management, charge transport and energy alignment with the chosen sensitizer. Indeed, over the years several attempts to optimize the aforementioned parameters by means of material shaping⁸⁻¹³, capping/mixture with other oxides¹⁴⁻¹⁹, or doping^{20,21} have been reported. Most of these studies dealt with the use of SnO₂ nanoparticles (SnO₂ NPs) of size spanning from about 6 to 140 nm, and were focused on understanding the role of light-matter interaction and charge transport through tin dioxide^{14,15,17,20-23}.

In the field of photosensitizers, phthalocyanines (Pcs) play a prominent role due to their excellent photo- and electrochemical stability and unique light harvesting capability in the red/NIR spectral regions, allowing the exploitation of a relevant portion of the solar photon flux that cannot be captured by other dyes²⁴. Such properties can be finely modulated by proper synthetic modifications that are relatively simple to perform^{25,26}. The optoelectronic properties of Pcs can indeed be effectively tuned by varying the organic substituents on the macrocyclic core, as this approach is successful in the modulation of the HOMO-LUMO energy levels and of the electron

¹Department of Information Engineering, University of Brescia, Via Valotti, 9 – 25131, Brescia, Italy. ²CNR-INO SENSOR Laboratory, via Branze, 45 – 25123, Brescia, Italy. ³Institute of Fundamental and Frontier Sciences, University of Electronic Science and Technology of China, Chengdu, 610054, P. R. China. ⁴Institut National de la Recherche Scientifique, Centre Énergie, Matériaux et Télécommunications, 1650 Boul. Lionel Boulet, Varennes, QC, J3X 1S2, Canada. ⁵Institute of Molecular Science and Technology, ISTM-CNR, Via Golgi, 19, 20133, Milano, Italy. ⁶Department of Chemical and Pharmaceutical Sciences, University of Ferrara, Via Borsari, 46, 44121, Ferrara, Italy. ⁷Division of Materials Science, Department of Engineering Sciences and Mathematics, Luleå University of Technology, 971 87, Luleå, Sweden. *email: isabella.concina@itu.se; gianluca.pozzi@istm.cnr.it

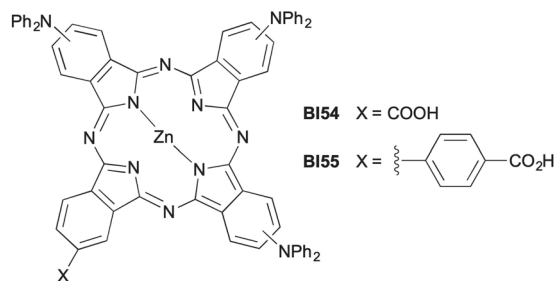


Figure 1. Peripherally substituted ZnPcs BI55 and BI54 bearing diphenylamino donors.

density distribution. Metallation of the Pc core, in particular coordination of Zn(II) that enables the existence of long-lived singlet excited states, is another strategy that proved of great utility for DSSCs applications²⁴. Because of this remarkable versatility, Pcs are appealing candidates as light harvesters in DSSCs, as witnessed by an impressive number of literature examples dealing with their use in combination with TiO₂ photoanodes^{27–32}. These studies also highlighted some issues seriously affecting the application of Pcs in TiO₂-based DSSCs, among which their aggregation on the titania surface³³, leading to the formation of never-ending dye layers on the ETM, jeopardizing the device functional performances due to enhanced exciton recombination³⁴. Unsymmetrically substituted Pcs bearing bulky, electron-donating groups on three of the four isoindole subunits which constitute the Pc macrocycle, and one or more electron-withdrawing groups able to interact with MOx on the fourth one have been designed to alleviate this issue^{27,28}. However, the addition of co-adsorbing agents (e.g. deoxycholic acid), competing with the sensitizer for anchoring sites on the TiO₂ surface and hindering interactions between Pc units, remains instrumental even with this favorable molecular pattern^{31,35}.

With these limitations in mind and following our continuous efforts to develop both ETMs and light harvesters for DSSCs, with particular focus on SnO₂ and ZnO as alternative materials for photoanodes^{36–38}, and on dyes capable of efficiently replacing the most commonly used Ru(II) complexes^{39–42}, we herein investigate the unprecedented use of Zn(II) complexes of unsymmetrically substituted push-pull Pcs (ZnPcs) as photosensitizers in DSSCs featuring SnO₂ NPs as ETM.

Results and Discussion

The most successful ZnPcs sensitizers reported so far are characterized by the concurrent presence of electron-rich aryloxy groups –OAr rotated with respect to the macrocycle plane and –COOH binding groups, according to a structural pattern essentially developed by a trial and error approach^{24,27,28}. Computational techniques were also applied to support a rational molecular design of unsymmetrical push-pull ZnPcs, strongly advocating the use of –NH₂, –NHR, –NR₂, NHPH or –NPh₂ donor groups instead of –OAr to improve DSSC functional performances^{43–45}. In order to test the validity of these predictions, we recently made available complex **BI54** (Fig. 1), the first example of unsymmetrical ZnPc bearing –NPh₂ donor groups.

While the measured optoelectronic parameters of **BI54** were in good agreement with computational models and potentially useful for DSSC applications, the photovoltaic performance of the dye when TiO₂ NPs were used as ETM disproved theoretical predictions⁴⁶. This inconsistency was ascribed, among others, to the problematic adsorption of **BI54** on TiO₂ NPs and to the possible shift of the CB of TiO₂ leading to a decreased charge injection efficiency from the excited state of the sensitizer. It was thus interesting to investigate the photovoltaic behavior of **BI54** in combination with a different ETM. On the other hand, the binding mode of unsymmetrical ZnPcs on MOx and their photovoltaic behavior are strongly influenced by the interposition of a linker between the Pc core and the anchoring group^{33,47–49}. We thus synthesized **BI55** (Fig. 1, see Supplementary Materials for details), an analog of **BI54** where the Pc core and the –COOH anchoring group are connected by an aryl ring, and tested the two ZnPcs in parallel as photosensitizers in DSSCs fabricated with SnO₂ NPs as ETM.

The energy levels of the HOMO-LUMO orbitals of **BI55** were assessed by electrochemical measurements combined with the analysis of the optical properties (Figures S1 and Table S1 in the Supplementary Materials). With HOMO and LUMO positioned at about –5.5 eV and –3.8 eV, respectively, and a typical UV-Vis absorption spectrum characterized by strong bands centered at 353 nm (Soret band) and 718 nm (Q band), the new dye satisfies the thermodynamic requirements for an effective use as light harvester in DSSCs, analogously to **BI54**⁴⁶.

Thanks to a favorable band alignment (sketched in Fig. 2), the use of SnO₂ should provide for a better driving force as for electron injection than that with TiO₂, given that the nanostructured MOx is properly designed for photogenerated charge transport and light scattering. SnO₂ is also expected to offer enhanced stability under UV exposure as compared with TiO₂ thanks to the wider band gap⁵⁰. Finally, SnO₂ is fit for coupling with NIR absorbing molecules, thus appearing the ideal candidate to be tested with both ZnPcs.

SnO₂ nanoparticles used as ETM were synthesized through a wet chemical approach using methanol as a solvent. In order to check the complete removal of methanol, as well as any residual surface hydroxyl groups, Fourier transform infrared spectroscopy was applied. The spectra pertaining to the material after the drying procedure in oven and to the metal oxide after the calcination are reported in the Supplementary Materials (Figure S2). SEM analysis of SnO₂ photoanodes (Fig. 3) evidences a homogenous deposition of the scattering layer over a wide area (Fig. 3a) and shows that the metal oxide is constituted of uniform spherical nanoparticles whose size is about 20 nm (Fig. 3b), as previously verified by XRD³⁶.

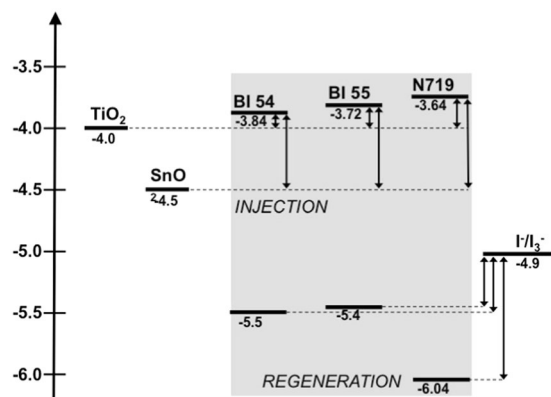


Figure 2. Energy band alignment of TiO_2 , SnO_2 and BI54, BI55 dyes. Commercial Ru(II) based dye N719 is reported for comparison purposes. Energy position of HOMO and LUMO of BI55 and BI54 have been obtained by electrochemical and optical analyses as described in the text.

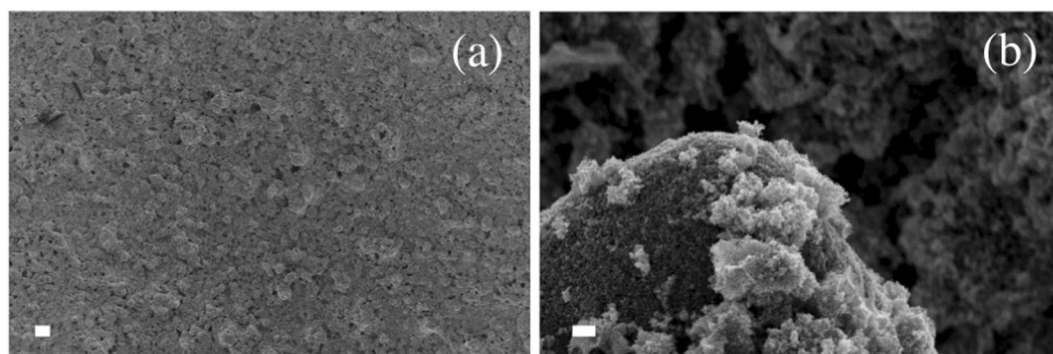


Figure 3. SEM images of SnO_2 nanoparticles based photoanodes. Scale bar: (a) 20 μm ; (b) 200 nm.

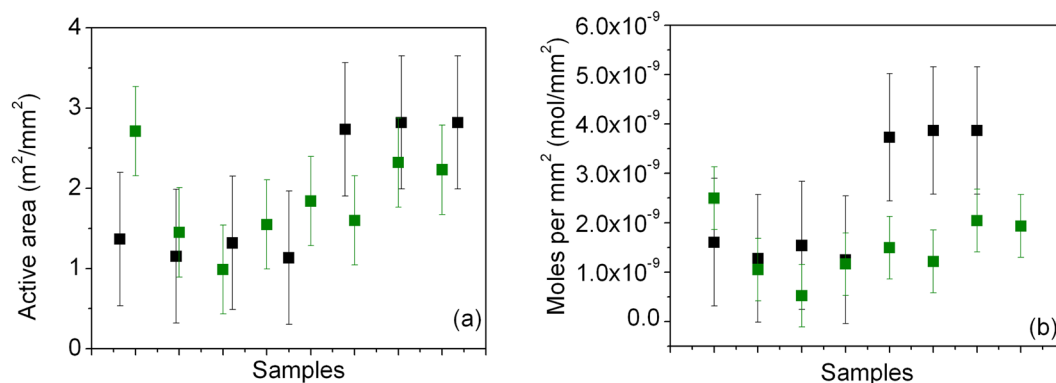


Figure 4. (a) Calculation of the active area per mm^2 featured by the SnO_2 (black markers) and TiO_2 (green markers) photoanodes. (b) Dye loading for the photoelectrodes based on SnO_2 (black markers) and TiO_2 (green markers) NPs.

Estimation of the active area per mm^2 of the SnO_2 photoelectrode has been performed by using the commercial Ru(II) based dye N719 as a molecular probe, considering a molecular area as high as 1.6 nm^2 for the dye⁵¹ and is reported in Fig. 4a, together with the data pertaining to TiO_2 photoelectrode, used as a benchmark.

An average value of about $1.25 \text{ m}^2/\text{mm}^2$ has been calculated for the SnO_2 NPs (TiO_2 photoanodes, composed of both transparent and scattering layers, i.e. with particles featuring diameters from 20 nm to 150–250 nm on average, featured a value as high as $1.84 \text{ m}^2/\text{mm}^2$). Active area is a critical parameter since it relates to dye loading capability, hence to the current that can be photogenerated in the solar energy converting device. Dye loading has been also evaluated by detaching the adsorbed dye N719 and found be about $2.45 \times 10^{-9} \text{ mol}/\text{mm}^2$ for SnO_2 photoanodes and $1.91 \times 10^{-9} \text{ mol}/\text{mm}^2$ for TiO_2 -based photoelectrodes (Fig. 4b). This is a relevant finding: it has

Entry No.	ETM/Dye	Additive	J_{sc} (mA/cm ²)	V_{oc} (V)	FF (%)	PCE (%)
1	SnO ₂ /N719	none	11.44	0.51	49	2.87
2	TiO ₂ /N719	none	11.61	0.74	63	5.38
3	SnO ₂ /BI54	none	0.355	0.07	19	0.005
4	SnO ₂ /BI54	DCA	2.605	0.18	27	0.13
5	SnO ₂ /BI54	DCA	2.38	327	41	0.32
6	SnO ₂ /BI55	DCA	1.11	260	38	0.11
7	TiO ₂ /BI54	DCA	1.376	0.54	58	0.43

Table 1. Functional parameters recorded for the dye sensitized solar cells presented in this work.

indeed been previously reported a significantly lower dye loading for SnO₂, ascribed to the more acidic nature of the SnO₂ surface (anatase TiO₂ presents the isoelectric point at pH 6.2, while for SnO₂ it is at pH 4–5)⁵². Usually the lower photocurrent featured by SnO₂-based DSSCs is then attributed to this difference in dye loading. However, in the present study, SnO₂ shows a dye uptake capability slightly higher than TiO₂ and, as we will see, this is reflected in the short circuit photocurrent density of the devices exploiting the two oxides as ETMs.

The functional parameters of various DSSCs based on SnO₂ as ETM and dyes **BI54** or **BI55** as light harvester are reported in Table 1, together with data obtained using the commercially available dye N719.

As previously mentioned, ZnPcs are usually subjected to aggregation due to π - π stacking, which leads to the formation of adsorbed multi-layers onto the MOx surface, detrimental for functional performances. We have recently demonstrated⁴⁶ that also **BI54** suffers of this issue on TiO₂ photoelectrodes and we verified the same in case of SnO₂. Indeed, solar converting device sensitized with dye **BI54** in the absence of co-adsorbing agents show very low functional performances (Entry 3 in Table 1 and Figure S1 in the Supplementary Materials). Deoxycholic acid (DCA) was thus added to the sensitizing mixture (50 mM), which resulted in enhancing all the functional parameters: J_{sc} increased of more than seven times, V_{oc} about 2.5 times and an increase of 26 times is recorded as for the photoconversion efficiency (entry 4 in Table 1). Thus, the addition of co-adsorbing agents acting as molecular spacers is confirmed as critical in order to effectively keep the dye molecules separated on the MOx surface and to avoid the formation of never-ending layers atop the ETM surface.

In order to assess the capability of SnO₂ NPs as ETM in DSSCs with respect to the more commonly used TiO₂, the behavior of devices with photoanodes sensitized with two different dyes, N719 and **BI54**, was investigated.

Figure 5a shows the J - V characteristics in dark and under simulated solar light of DSSCs sensitized with N719, where the ETM is either TiO₂ (green lines) or SnO₂ (black lines). Functional parameters are reported in Table 1, entries 1 and 2).

When the commercial Ru-based dye N719 is used as light harvester, a higher V_{oc} value is recorded for the TiO₂-based device (740 mV) compared with the solar cell working with SnO₂ as ETM (510 mV), as expected, while comparable short circuit current is observed (11.61 vs. 11.44 mA/cm² for TiO₂ and SnO₂ photoanodes, respectively). Electron lifetime (Fig. 5b) is found to be slightly longer for the cell based on SnO₂.

It is worth noting that the performances of the present bare (i.e. without any surface treatment aimed at reducing back recombination between the MOx CB and the electrolyte) SnO₂-based DSSCs sensitized with N719 are much higher than those previously reported for other bare SnO₂ photoanodes, as it can be seen in Table 2.

Open circuit photovoltage value observed in the present work is the highest recorded for SnO₂-based DSSCs where neither TiO₂ buffer layer is applied to the conductive substrate nor TiCl₄ post treatment is used to cap the SnO₂ ETM. This outcome is of extreme relevance: it indicates, indeed, that the synthesized SnO₂ NPs feature an appropriate charge transport skill, with reduced exciton recombination, as compared with previously investigated photoanodes based on the same MOx.

When dye **BI54** is applied as light harvester (Fig. 6c,d), the observed open circuit photovoltage is still higher for TiO₂ (540 mV) than for SnO₂ (180 mV), for which, however, it is reduced beyond the expectations. On the contrary, short circuit current density is almost two times higher when SnO₂ is applied as ETM (2.605 mA/cm² vs. 1.376 mA/cm² recorded for TiO₂-based DSSC). One of the advantages of SnO₂ over TiO₂ is the higher electron mobility: mobility reported for SnO₂ ($\mu_e \approx 250$ cm²V⁻¹s⁻¹ for SnO₂ single crystal⁵³ and $\mu_e \approx 125$ cm²V⁻¹s⁻¹ for SnO₂ nanostructures⁵⁴) is order of magnitude higher than the one reported for TiO₂ ($\mu_e < 1$ cm²V⁻¹s⁻¹ for TiO₂ single crystal⁵⁵). However, this higher mobility is of no help with Ru-based light harvesters, as widely shown in literature, while it is capable of spurring the photogenerated current when a light harvester with specifically designed feature is applied.

Electron lifetime appears slightly longer for the TiO₂-based device (Fig. 6c). The Reader should however be aware that a longer electron lifetime may also be correlated to the presence of charges trapped in undesired surface states, which are of no use in converting the solar light.

Analysis of J - V characteristics in dark provides useful information on the origin of the seemingly inconsistent behavior of the two MOx. We should herein remind that V_{oc} should ideally match the difference in energy between the conduction band (CB) of the ETM and the standard redox potential of the electrolyte couple (the iodine/triiodine in the systems analyzed here). Such view well explains the difference in V_{oc} observed for TiO₂- and SnO₂-based DSSCs exploiting dye N719 as a dye (see the energy scheme reported in Fig. 2), but it is no longer satisfactory when **BI54** is instead used. J - V characteristics in dark (reported as dotted lines for both MOx and both dyes in Fig. 6a,c) show an increased dark current for SnO₂-based devices, irrespectively of the used dye. The difference in dark current is moderate for devices sensitized with dye N719 (Fig. 6a): for both cells dark current onset is around 350 mV. This difference is however more pronounced in DSSCs sensitized with dye **BI54** (Fig. 6c),

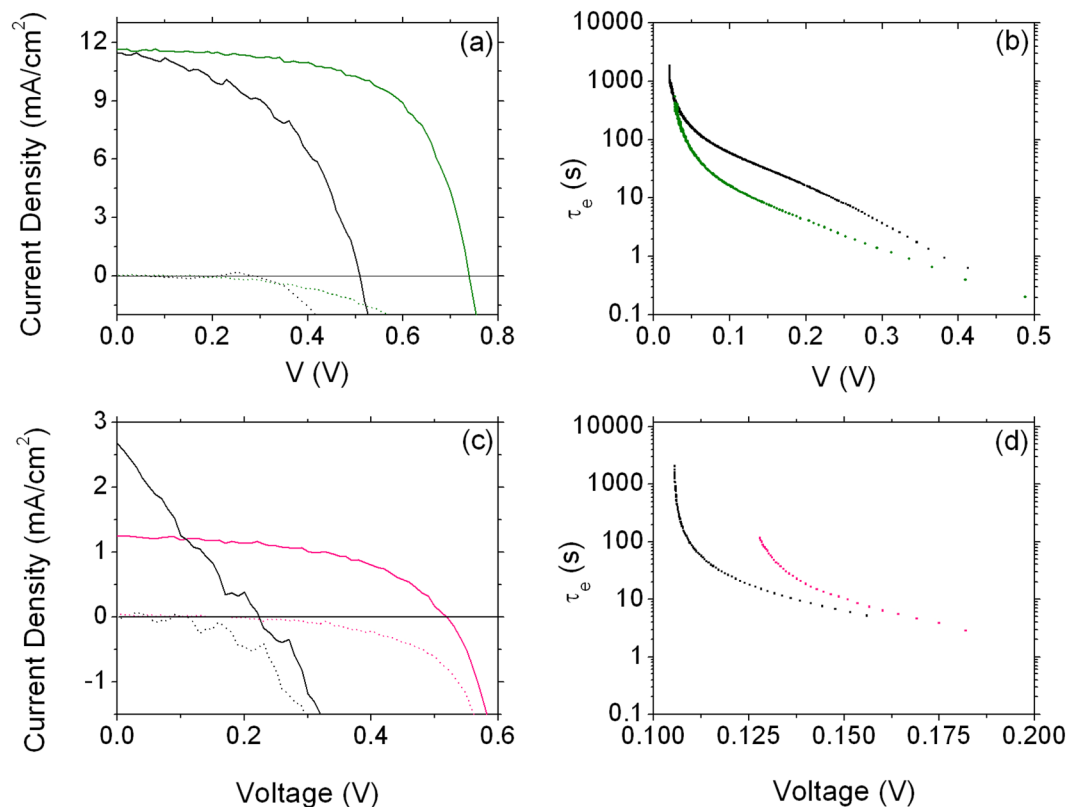


Figure 5. Comparison of the performance of TiO₂ and SnO₂ as ETM for DSSCs. (a) and (c) = J - V characteristics under simulated solar light (solid lines) and in dark (dashed lines); (b) and (d) = electron lifetime. (a) and (b): N719 is used as light harvester. (c) and (d): BI54 is used as light harvester. Black line: SnO₂; green and pink lines: TiO₂.

Photoanode	Notes	J_{sc} (mA/cm ²)	V_{oc} (mV)	FF (%)	PCE (%)	Reference
Bare SnO ₂	20 nm NPs	11.44	510	49	2.87	This work
Bare SnO ₂	20 nm NPs SnO ₂ blocking layer on FTO glass	~10	230	35	0.76	17
Bare SnO ₂	15 nm + 140 nm NPs	6.4	480	40	1.2	15
Bare SnO ₂	18 nm NPs	1.7	470	40	0.5	22
Bare SnO ₂	7.92 nm NPs	5.76	445	49	1.26	19
Bare SnO ₂	Hollow spheres (20 nm NPs)	6.40	390	34	0.86	8
	Hollow spheres (20 nm NPs) + TiCl ₄ treatment	14.59	765	54	6.02	8
Bare SnO ₂	6.5 nm NPs	6.1	292	37	0.66	21
Bare SnO ₂	18 nm NPs	5.7	320	27	0.51	16
	Hierarchical octahedral	6.84	543	56	2.07	9
	Hierarchical octahedral + TiO ₂ blocking layer	10.96	604	47.9	3.17	9
Bare SnO ₂	15 nm NPs	2.5	335	–	–	14
Commercial SnO ₂ NPs	80–100 nm [‡]	6.71	330	47.96	1.07	20
SnO ₂ mesoporous microspheres	Microsphere sizes 1.2–1.5 μm (composed of packed nanobeads, 10–15 nm)	10.08	400	54.44	2.31	20
Bare SnO ₂	8–20 nm NPs	3.62	340	30.20	0.36	23

Table 2. Functional parameters of SnO₂-based DSSCs reported in literature. [‡] Sizes inferred by SEM images reported in the supporting information of ref. 20.

for which the onset moved below 200 mV. The dark current in solar cells comes from charge recombination: an enhancement of dark current is then associated to a faster recombination²², which is usually reflected in lower open circuit voltage values, as it is in the present cases. Given that the two devices have exactly the same structure but for the sensitizer, this effect is to be correlated with the nature of the ZnPc light harvester, which apparently is inhibiting the charge transport more than dye N719. The differences in the onset of dark current recorded for dye N719 and BI54 can be ascribed to the skill of N719 in partially blocking the recombination at the FTO|electrolyte

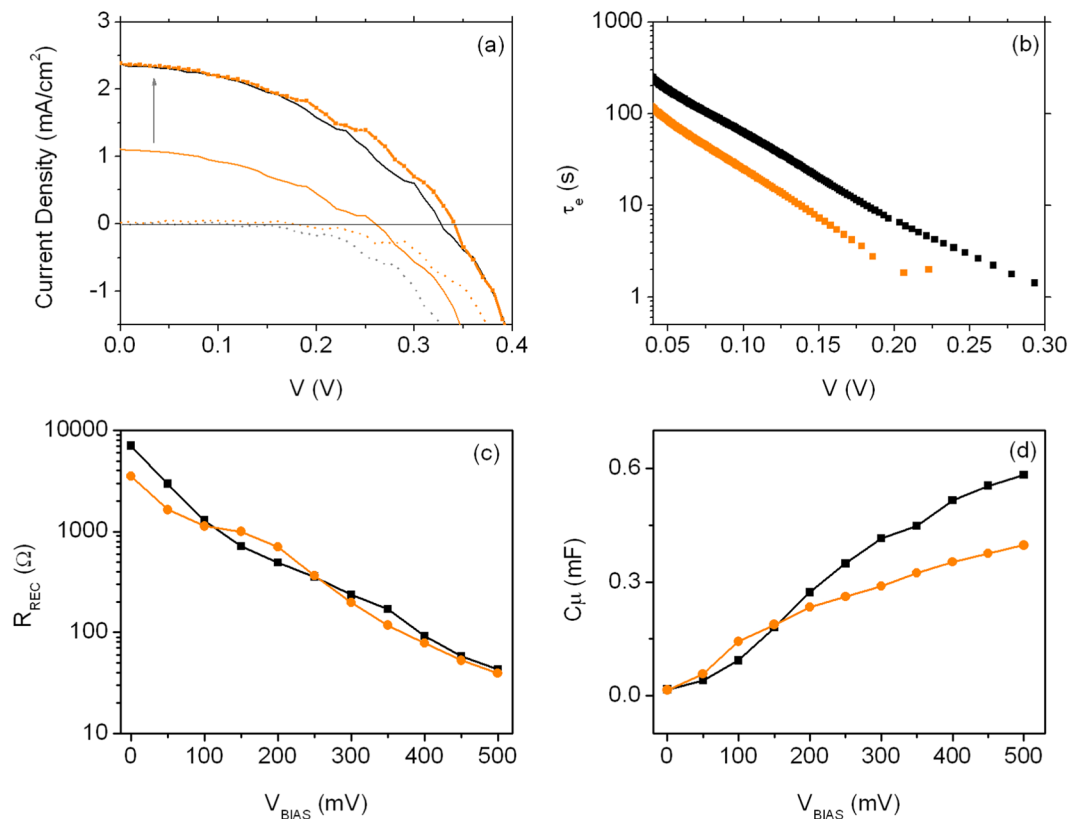


Figure 6. Comparison between DSSC sensitized with BI55 (orange line and markers) and BI54 (black line and markers). (a) J - V characteristics (solid lines: simulated solar light; dotted line: dark); (b) electron lifetime; (c) recombination resistance; (d) chemical capacitance.

interface⁵⁶, which is not featured by the ZnPc **BI54**. One of the reasons why SnO₂ is investigated as alternative ETM to TiO₂ in excitonic solar cells is, as mentioned, the higher electron mobility featured by this MOx. However, it should not be neglected that this higher electron mobility might also result in enhanced recombination, leading to a more pronounced electron-hole recombination.

The most relevant photovoltaic parameters of SnO₂-based DSSCs sensitized with ZnPCs **BI55** or **BI54** are summarized in Fig. 6 (functional parameters are reported in Table 1, entries 5 and 6).

Interestingly the shapes of J - V characteristics are quite similar and suggest no difference between the resistances of the two devices (shunt resistance, R_{SH} , and series resistance, R_S). Since the values for V_{OC} only differ for 67 mV (260 mV and 327 mV for sensitizer **BI55** and sensitizer **BI54**, respectively), a different adsorption mode of the dyes to the surface of oxide might be responsible of the difference in term of J_{SC} . The Fermi level E_F and the electric field that assists the injection of the charges are possibly similar for the two devices and the density of the charge is lower in the case of **BI55**.

Also in this case, dark J - V characteristics bring useful information to explain the difference in performances. The device sensitized with ZnPc **BI55** shows an enhanced dark current, which, accordingly to what mentioned above, suggests a reduced skill of the dye in blocking the recombination at the FTO|electrolyte interface. By equaling the short circuit currents⁵⁷, i.e. the charge injection (orange markers in Fig. 6a), it is possible to observe that the DSSCs work in the same way. This strongly suggests that the limiting factor in the **BI55**-sensitized device is the charge injection from the LUMO to the SnO₂ CB. The EIS analysis applied to these two cells confirms this hypothesis (Fig. 6c,d). The two devices show no differences in R_{REC} (Fig. 6c), while the trends of C_{μ} (Fig. 6d) suggests a downward of the CB for the oxide sensitized with BI54, as previously reported⁴⁶. Indeed, the slope of C_{μ} is different when the two ZnPCs are applied: C_{μ} pertaining to the device sensitized with ZnPc **BI55** is less steep as compared with that observed in case of **BI54**, indicating a beneficial and better capping of the SnO₂ trap states by this latter. We have reported similar observations when TiO₂ is applied as ETM and comparison is made between the dyes N719 and **BI54**⁴⁶. Also in that case, poor injection was found responsible for the lower functional performances.

Conclusions

We presented a study on the use of two unsymmetrically substituted ZnPCs as light harvesters in DSSCs exploiting either TiO₂ or SnO₂ nanoparticles as ETM.

Investigated molecules have been especially designed to fulfil the requirements identified by computational models as for energy level alignment between their LUMO and the MOx CB, good charge injection and absorption range extended to the infrared portion of the solar spectrum.

On the other hand, SnO₂ nanoparticles developed in the present study have shown very nice performances when the commercial Ru(II)-based dye N719 is applied as sensitizer as compared with previously reported tin dioxide photoanodes, featuring a photogenerated current density comparable with that observed with TiO₂ photoanodes and very good open circuit photovoltage.

Despite the excellent preconditions for both components, device functional performances proved to be below the expectations (less than 1% as for photoconversion efficiency). Main reasons behind this outcome have been identified in the poor charge injection from the excited ZnPcs to the CB of SnO₂ and low capability of ZnPcs in contributing to block the recombination at the FTO|electrolyte interface. As in the case of TiO₂-based DSSCs, our findings also confirm the ease of aggregation of ZnPcs on the MOx surface its negative impact on the device performance. We will thus focus our efforts on improving the performance of SnO₂-based devices through specific modifications of the substitution pattern of the phthalocyanine ring, according to a strategy recently demonstrated in the case of perovskite solar cells featuring ZnPcs as hole transporting materials⁵⁸.

While hypotheses built up by molecular modelling are useful hints for the design of new photosensitizers, this work confirms that a thorough analysis of the results obtained through experimental tests remains crucial for further structural modifications and refinements. Indeed, many parameters play a relevant role in the working mechanism of a solar energy converting devices and unexpected factors may reveal more critical than expected.

Methods

Dye-sensitized solar cells. *SnO₂ nanoparticles synthesis.* In a round bottomed flask 1.2 ml SnCl₄ were dissolved in 100 ml of methanol. After the fumes had disappeared, 4 ml NH₄OH (30% in water) were added dropwise in about 10 minutes. As soon as NH₄OH was added, a white flocculate appeared in the reaction mixture. Mixture was let reacting for about 20 minutes at room temperature, and then the solvent was slowly evaporated at 80 °C in an oven (6–7 h). The raw product was then annealed at 450 °C for 2 h under air atmosphere. All chemicals were purchased from Sigma-Aldrich and used without any further purification.

SnO₂ paste preparation. SnO₂ paste was prepared by mixing 0.8 g of SnO₂ nanoparticles powder with ethyl cellulose (0.7 g) and α-terpineol (1.5 ml), in ethanol/water dispersion medium (8/3.5, V/V). The mixture was kept under vigorous stirring overnight to obtain a homogenous paste suitable for tape casting.

Photoanode preparation. TiO₂ pastes (Dyesol 20 nm anatase nanoparticles paste 18NR-T and WER2-O, composed of anatase nanoparticles with diameter between 150 and 250 nm) were purchased from Dyesol. The redox electrolyte was composed of 0.1 M LiI, 0.05 M I₂, 0.6 M 1,2-dimethyl-3-*n*-propylimidazolium iodide, and 0.5 M 4-*tert*-butylpyridine dissolved in acetonitrile.

The TiO₂ and SnO₂ paste were deposited onto FTO glass (sheet resistance 10 Ω/□) by tape casting technique. The paste was dried 15 min at ambient conditions and then fired on hot plate for 6 min (125–130 °C) for the TiO₂ based photoanodes and 10 min at ambient conditions and then fired on hot plate for 45 min (100 °C) for SnO₂ based photoanodes. In the case of TiO₂ paste two layers of transparent TiO₂ (18NR-T) and one of scattering TiO₂ (WER2-O) were deposited.

All the samples were finally annealed at 450 °C for 30 min under ambient atmosphere. Photoanode thickness was evaluated by stylus profilometry and found about 15 μm.

The sensitization of photoanodes was performed for 5 hours in dark condition using solutions containing 0.5 mM N719 in ethanol and 0.17 mM BI54 or BI55 in dichloromethane.

Device assembly. DSSCs were fabricated using dye sensitized oxide photoanodes and platinized FTO glass as a counter electrode (5 nm Pt thin film deposited by sputtering) with 60 μm-thick plastic spacers (Surlin from Solaronix). The I₃⁻/I⁻ redox couple electrolyte was composed of 0.1 M LiI, 0.05 M I₂, 0.6 M 1,2-dimethyl-3-*n*-propylimidazolium iodide, and 0.5 M 4-*tert*-butylpyridine dissolved in acetonitrile.

Scanning electron microscopy analysis was carried out in a LEO 1525 FE-SEM.

Dye loading quantification and metal oxide surface area evaluation were performed by spectrophotometry, detaching the absorbed dye N719 by using a 0.1 M NaOH aqueous solution and recording the UV-Vis absorption spectra in a T80 spectrophotometer (PG Instruments) after building up a calibration curve with standard solutions; quartz cuvettes were used (1 cm optical path).

The current–voltage (I–V) characteristics of the fabricated cells were measured without masking by using a Keithley 2400 SourceMeter under simulated sunlight using an ABET2000 solar simulator at AM 1.5 G (100 mW cm⁻²) calibrated using a reference silicon cell. The electrochemical impedance spectroscopy (EIS) was carried out in dark conditions using a SOLARTRON 1260 A Impedance/Gain-Phase Analyzer, with an AC signal 20 mV in amplitude, in the frequency range between 100 mHz and 300 kHz. An external bias was applied from 0 to 100 mV above the V_{OC}.

Electron lifetime of the photogenerated charges present in the CB of the dyed semiconductor is calculated from open circuit voltage decay using the following equation:⁵⁹

$$\tau_n = - \frac{k_B T}{e} \left(\frac{dV_{OC}}{dt} \right)^{-1}$$

where $k_B T$ is the thermal energy, e is the positive elementary charge.

Received: 11 June 2019; Accepted: 23 December 2019;

Published online: 24 January 2020

References

- Hagfeldt, A., Boschloo, G., Sun, L., Kloo, L. & Pettersson, H. Dye-sensitized solar cells. *Chem. Rev.* **110**, 6595–6663 (2010).
- Shaikh, J. S. *et al.* Nanoarchitectures in dye-sensitized solar cells: metal oxides, oxide perovskites and carbon-based materials. *Nanoscale* **10**, 4987–5034 (2018).
- Concina, I. & Vomiero, A. Metal oxide semiconductors for dye- and quantum-dot-sensitized solar cells. *Small* **11**, 1744–1774 (2015).
- Zhuang, S. *et al.* Cu modified ZnO nanoflowers as photoanode material for highly efficient dye sensitized solar cells. *Electrochim. Acta* **294**, 28–37 (2019).
- Xie, F., Wang, J., Li, Y., Dou, J. & Wei, M. One-step synthesis of hierarchical SnO₂/TiO₂ composite hollow microspheres as an efficient scattering layer for dye-sensitized solar cells. *Electrochim. Acta* **296**, 142–148 (2019).
- Patil, J. V. *et al.* Influence of reduced graphene oxide-TiO₂ composite nanofibers in organic indoline DN350 based dye sensitized solar cells. *Synth. Met.* **256**, 116146 (2019).
- Shalini, S. *et al.* Status and outlook of sensitizers/dyes used in dye sensitized solar cells (DSSC): a review. *Int. J. Energy Res.* **40**, 1303–1320 (2016).
- Wang, H. *et al.* SnO₂ hollow nanospheres enclosed by single crystalline nanoparticles for highly efficient dye-sensitized solar cells. *Cryst. Eng. Comm.* **14**, 5177–5181 (2012).
- Wang, Y.-F. *et al.* Hierarchical tin oxide octahedra for highly efficient dye-sensitized solar cells. *Chem. Eur. J.* **16**, 8620–8625 (2010).
- Elumalai, N. K., Jose, R., Archana, P. S., Chellappan, V. & Ramakrishna, S. Charge transport through electrospun SnO₂ Nanoflowers and nanofibers: role of surface trap density on electron transport dynamics. *J. Phys. Chem. C* **116**, 22112–22120 (2012).
- Shang, G. *et al.* Facile synthesis of mesoporous tin oxide spheres and their applications in dye-sensitized solar cells. *J. Phys. Chem. C* **116**, 20140–20145 (2012).
- Song, H. *et al.* A simple self-assembly route to single crystalline SnO₂ nanorod growth by oriented attachment for dye sensitized solar cells. *Nanoscale* **5**, 1188–1194 (2013).
- Tarini, M., Prakash, N., Mathar Sahib, I. K. M. & Hayakawa, Y. Novel sugar apple-shaped SnO₂ microspheres with light scattering effect in dye-sensitized solar cell application. *IEEE J. Photolt.* **7**, 1050–1057 (2017).
- Tennakone, K., Kumara, G. R. R. A., Kottegoda I. R. M., Perera, V. P. S. An efficient dye-sensitized photoelectrochemical solar cell made from oxides of tin and zinc. *Chem. Commun.*, 15–16 (1999).
- Kay, A. & Grätzel, M. Dye-Sensitized Core-Shell Nanocrystals: Improved efficiency of mesoporous tin oxide electrodes coated with a thin layer of an insulating oxide. *Chem. Mater.* **14**, 2930–2935 (2002).
- Chappel, S., Chen, S.-G. & Zaban, A. TiO₂-coated nanoporous SnO₂ electrodes for dye-sensitized solar cells. *Langmuir* **18**, 3336–3342 (2002).
- Prasittichai, C. & Hupp, J. T. Surface modification of SnO₂ photoelectrodes in dye-sensitized solar cells: significant improvements in photovoltage via Al₂O₃ atomic layer deposition. *J. Phys. Chem. Lett.* **1**, 1611–1615 (2010).
- Desai, U. V., Xu, C., Wu, J. & Gao, D. Hybrid TiO₂–SnO₂ nanotube arrays for dye-sensitized solar cells. *J. Phys. Chem. C* **117**, 3232–3239 (2013).
- Park, N.-G., Kang, M. G., Kim, K. M., Ryu, K. S. & Chang, S. H. Morphological and photoelectrochemical characterization of core-shell nanoparticle films for dye-sensitized solar cells: Zn-O type shell on SnO₂ and TiO₂ cores. *Langmuir* **20**, 4246–4253 (2004).
- Li, Z. *et al.* Versatile nanobead-scaffolded N-SnO₂ mesoporous microspheres: one-step synthesis and superb performance in dye-sensitized solar cell, gas sensor, and photocatalytic degradation of dye. *J. Mater. Chem. A* **1**, 524–531 (2013).
- Park, N.-G., Gu Kang, M., Sun Ryu, K., Man Kim, K. & Ho Chang, S. Photovoltaic characteristics of dye-sensitized surface-modified nanocrystalline SnO₂ solar cells. *J. Photochem. Photobiol. A: Chemistry* **161**, 105–110 (2004).
- Green, A. N. M., Palomares, E., Haque, S. A., Kroon, J. M. & Durrant, J. R. Charge transport versus recombination in dye-sensitized solar cells employing nanocrystalline TiO₂ and SnO₂ films. *J. Phys. Chem. B* **109**, 12525–12533 (2005).
- Pereira, M. S., Lima, F. A. S., Silva, C. B., Freire, P. T. C. & Vasconcelos, I. F. Structural, morphological and optical properties of SnO₂ nanoparticles obtained by a proteic sol-gel method and their application in dye-sensitized solar cells. *J. Sol-Gel Sci. Technol.* **84**, 206–213 (2017).
- Urbani, M., Ragoussi, M.-E., Nazeeruddin, M. K. & Torres, T. Phthalocyanines for dye-sensitized solar cells. *Coord. Chem. Rev.* **381**, 1–64 (2019).
- Wang, A., Long, L. & Zhang, C. Synthesis of unsymmetrical phthalocyanines: a brief overview. *Tetrahedron* **68**, 2433–2451 (2012).
- Ragoussi, M.-E. & Torres, T. Modern synthetic tools toward the preparation of sophisticated phthalocyanine-based photoactive systems. *Chem. Asian J.* **9**, 2676–2707 (2014).
- Singh, V. K., Kanaparthi, R. K. & Giribabu, L. Emerging molecular design strategies of unsymmetrical phthalocyanines for dye-sensitized solar cell applications. *RSC Adv.* **4**, 6970–6984 (2014).
- Martín-Gomis, L., Fernández-Lázaro, F. & Sastre-Santos, Á. Advances in phthalocyanine-sensitized solar cells (PcSSCs). *J. Mater. Chem. A* **2**, 15672–15682 (2014).
- Tejerina, L., Martínez-Díaz, M. V., Nazeeruddin, M. K., Graetzel, M. & Torres, T. Role of the bulky aryloxy group at the non-peripheral position of phthalocyanines for dye sensitized solar cells. *ChemPlusChem* **82**, 132–135 (2017).
- Suanzes Pita, J. *et al.* Pyridyl- and picolinic acid substituted zinc(II) phthalocyanines for dye-sensitized solar cells. *ChemPlusChem* **82**, 1057–1061 (2017).
- Martín-Gomis, L., Parejo, C., Alvarez, J. C., Fernández-Lázaro, F. & Sastre-Santos, Á. L. Dye sensitized solar cells (DSSCs) based on bulky tert-octylphenoxy-carboxyphenyl substituted phthalocyanine without the presence of co-adsorbents. *Inorganica Chimica Acta* **468**, 327–333 (2017).
- Kimura, M. *et al.* Carbazole-fused zinc(II)-phthalocyanine sensitizers. *Asian J. Org. Chem.* **6**, 544–550 (2017).
- Matsuzaki, H. *et al.* Dye aggregation effect on interfacial electron-transfer dynamics in zinc phthalocyanine-sensitized solar cells. *J. Phys. Chem. C* **118**, 17205–17212 (2014).
- Zhang, L. & Cole, J. M. Dye aggregation in dye-sensitized solar cells. *J. Mater. Chem. A* **5**, 19541–19559 (2017).
- Yum, J. H. *et al.* Effect of coadsorbent on the photovoltaic performance of zinc phthalocyanine-sensitized solar cells. *Langmuir* **24**, 5636–5640 (2008).
- Milan, R. *et al.* ZnO@SnO₂ engineered composite photoanodes for dye sensitized solar cells. *Scientific Reports* **5**, 14523 (2015).
- Memarian, N. *et al.* Hierarchically assembled ZnO nanocrystallites for high-efficiency dye-sensitized solar cells. *Angew. Chem. Int. Ed.* **50**, 12321–12325 (2011).
- Selopal, G. S. *et al.* Effect of blocking layer to boost photoconversion efficiency in ZnO dye-sensitized solar cells. *ACS Appl. Mater. Interfaces* **6**, 11236–11244 (2014).
- Selopal, G. S. *et al.* Metal-free organic dyes for TiO₂ and ZnO dye-sensitized solar cells. *Scientific Reports* **6**, 18756 (2016).
- Pecnikaj, I. *et al.* Fluorous molecules for dye-sensitized solar cells: synthesis and properties of di-branched, di-anchoring organic sensitizers containing fluorene subunits. *New J. Chem.* **41**, 7729–7738 (2017).
- Tortelli, S. *et al.* Property tuning in unsymmetrical alkoxy zinc phthalocyanines by introduction of perfluoro-tert-butoxy end groups. *J. Fluorine Chem.* **188**, 110–116 (2016).

42. Pozzi, G. *et al.* Synthesis and photovoltaic applications of a 4,4'-spirobi[cyclopenta[2,1-b;3,4-b']dithiophene]-bridged donor/acceptor Dye. *Org. Lett.* **15**, 4642–4265 (2013).
43. Yang, L. *et al.* Theoretical design and screening of panchromatic phthalocyanine sensitizers derived from TT1 for dye-sensitized solar cells. *J. Mol. Graphics Modell.* **34**, 1–9 (2012).
44. Yang, L. *et al.* Substituent effects on zinc phthalocyanine derivatives: a theoretical calculation and screening of sensitizer candidates for dye-sensitized solar cells. *J. Mol. Graphics Modell.* **38**, 82–89 (2012).
45. Linares-Flores, C., Mendizabal, F., Arratia-Pérez, R., Inostroza, N. & Orellana, C. Substituents role in zinc phthalocyanine derivatives used as dye-sensitized solar cells. A theoretical study using Density Functional Theory. *Chem. Phys. Lett.* **639**, 172–177 (2015).
46. Milan, R. *et al.* Dye-sensitized solar cells based on a push-pull zinc phthalocyanine bearing diphenylamine donor groups: computational predictions face experimental reality. *Scientific Reports* **7**, 15675 (2017).
47. Kimura, M. *et al.* Molecular design rule of phthalocyanine dyes for highly efficient near-IR performance in dye-sensitized solar cells. *Chem. Eur. J.* **19**, 7496–7502 (2013).
48. Ragoussi, M. E. *et al.* Sterically hindered phthalocyanines for dye-sensitized solar cells: influence of the distance between the aromatic core and the anchoring group. *Chem. Phys. Chem.* **15**, 1033–1036 (2014).
49. Ikeuchi, S., Agrawal, M., Ezoe, S., Mori, S. & Kimura, M. Enhanced Charge separation efficiency in pyridine-anchored phthalocyanine-sensitized solar cells by linker elongation. *Chem. Asian J.* **10**, 2347–2351 (2015).
50. Fonstad, C. G. & Rediker, R. H. Electrical properties of high quality stannic oxide crystals. *J. Appl. Phys.* **42**, 2911–2918 (1971).
51. Grätzel, M. Molecular photovoltaics that mimics photosynthesis. *Pure Appl. Chem.* **73**, 459–467 (2001).
52. Parks, G. A. The isoelectric points of solid oxides, solid hydroxides, and aqueous hydroxo complex systems. *Chem. Rev.* **65**, 177–198 (1965).
53. Jarzebski, M. & Marton, J. P. Physical properties of SnO₂ materials. *J. Electrochem. Soc.* **123**, 299C (1976).
54. Arnold, M. S., Avouris, P., Pan, Z. W. & Wang, Z. L. Field-effect transistors based on single semiconducting oxide nanobelts. *J. Phys. Chem. B* **107**, 659–663 (2003).
55. Hendry, E., Koeberg, M., O'Regan, B. & Bonn, M. Local field effects on electron transport in nanostructured TiO₂ revealed by terahertz spectroscopy. *Nano Lett.* **6**, 755–759 (2006).
56. Ito, S., *et al.* Control of dark current in photoelectrochemical (TiO₂/I₂-I₃⁻) and dye-sensitized solar cells, *Chem. Commun.* 4351–4353 (2005).
57. Barea, E. M. *et al.* Energetic factors governing injection, regeneration and recombination in dye solar cells with phthalocyanine sensitizers. *Energy Environ. Sci.* **3**, 1985–1994 (2010).
58. Cho, K. T. *et al.* Perovskite solar cells: 18% efficiency using Zn(II) and Cu(II) octakis(diarylamine)phthalocyanines as hole-transporting materials. *ACS Appl. Energy Mater.* **2**, 6195–6199 (2019).
59. Zaban, A., Greenshtein, M. & Bisquert, J. Determination of the electron lifetime in nanocrystalline dye solar cells by photovoltage decay measurements. *Chem. Phys. Chem.* **4**, 859–864 (2003).

Acknowledgements

The present work has been supported by the CNR/Regione Lombardia project “Integrated Zero Emission Buildings”. IC thanks VINNOVA under the VINNMER Marie Curie Incoming project “Light Energy” (Li-En) No. 2015-01513 for partial funding. Open access funding provided by Lulea University of Technology.

Author contributions

R.M. and G.S.S. fabricated the solar cells and tested them. M.C and S.O. contributed to the synthesis of the light harvesters. R.B. and S.C. carried out the cyclic voltammetry to calculate the energy values of HOMO and LUMO of metallorganic molecules. I.C. and G.P. designed the overall study, characterized the phthalocyanines and the electron transport material and wrote the manuscript.

Competing interests

The authors declare no competing interests.

Additional information

Supplementary information is available for this paper at <https://doi.org/10.1038/s41598-020-58310-1>.

Correspondence and requests for materials should be addressed to I.C. or G.P.

Reprints and permissions information is available at www.nature.com/reprints.

Publisher's note Springer Nature remains neutral with regard to jurisdictional claims in published maps and institutional affiliations.



Open Access This article is licensed under a Creative Commons Attribution 4.0 International License, which permits use, sharing, adaptation, distribution and reproduction in any medium or format, as long as you give appropriate credit to the original author(s) and the source, provide a link to the Creative Commons license, and indicate if changes were made. The images or other third party material in this article are included in the article's Creative Commons license, unless indicated otherwise in a credit line to the material. If material is not included in the article's Creative Commons license and your intended use is not permitted by statutory regulation or exceeds the permitted use, you will need to obtain permission directly from the copyright holder. To view a copy of this license, visit <http://creativecommons.org/licenses/by/4.0/>.

© The Author(s) 2020